Aerosol size characteristics over the Arabian Sea and Indian Ocean: Extensive sub-micron aerosol loading in the northern hemisphere

K. Krishna Moorthy[*§], Preetha S. Pillai[*], Auromeet Saha[#] and K. Niranjan[#]

*Space Physics Laboratory, Vikram Sarabhai Space Centre, Thiruvananthapuram 695 022, India
#Department of Physics, Andhra University, Visakhapatnam 530 003, India

Aerosol size characteristics and columnar loading are deduced from spectral optical depths estimated over the Arabian Sea and south-western Indian Ocean, using a 10 channel multi-wavelength solar radiometer (MWR) on board the cruise #133 of ORV *Sagar Kanya* during the First Field Phase (FFP-98) of the Indian Ocean Experiment (INDOEX). The columnar size distributions showed a clear and consistent bimodal nature over the oceanic areas of the northern hemisphere (or due north of the inter-tropical convergence zone (ITCZ)) with a sub-micron accumulation mode at ~ 0.05 μm and a coarse particle mode at ~ 1 μm; both are attributed to different source mechanisms. There is a rapid decrease in aerosol mass loading as one moves to remote oceanic regions from the coast. Over the pristine environment, on the south of the ITCZ, the accumulation mode tends to vanish leading to broad unimodal distributions; the mass loading becomes $< \sim 70$ mg m^{-2} column. Aerosol size characteristics show an extensive increase in the relative abundance of sub-micron ($r < 0.5$ μm) aerosols in the northern hemisphere. The concentration of these is highest in the coastal and interior regions of the north-western Arabian Sea and decrease rapidly as one moves to the Indian Ocean. The results are discussed based on different aerosol generation mechanisms and the possible transport through air trajectories.

PREVAILING winds transport continental aerosols, generated directly from natural and anthropogenic activities (wind blown mineral dust, industrial and urban effluvia) and indirectly from gas phase reactions of anthropogenic low volatile vapours in the atmosphere, over to oceanic environments. Such aerosol transport is a major perturbing component of the marine aerosol system[1–5]. Impact of aerosol components of possible continental origin in influencing physical and optical properties of pure oceanic aerosols have been reported by various researchers[5–7]. The inter-tropical convergence zone (ITCZ) is a region where the two opposing flows, one from the northern continents and the other from southern pristine ocean, meet causing a convergence and deep convection. The seasonal movement of the ITCZ causes the polluted continental air to overlap with the purer oceanic environment during favourable seasons (the Indian winter, for example); such movement cleanses the continental air, but also pollutes the oceanic air[7,8]. The finer aerosols (or the sub-micron aerosols), which are mainly generated over the land by gas phase reactions of industrial and urban effluents (mainly sulphates, and nitrates and soot), contribute significantly to pollution because of their longer residence time in the atmosphere[2,9]. One of the objectives of the INDOEX programme is to assess the role of these continental aerosols in modifying the features of the marine boundary layer (MBL) and the role of ITCZ in transporting them horizontally and vertically[8]. In this paper, we present an investigation of the changes in aerosol size distributions and number concentrations over the Arabian Sea and the Indian Ocean and their relation to the ITCZ; the data come from on board measurements from the cruise # 133 of *Sagar Kanya* during the First Field Phase (FFP-98) of the INDOEX.

Basic data

The basic data used for this study are the aerosol spectral optical depth ($\tau_{p\lambda}$) obtained at 10 narrow wavelength bands using a multiwavelength radiometer (MWR) onboard the cruise, at various oceanic locations. The details of the cruise track, instruments, the wavelengths involved and estimation of $\tau_{p\lambda}$ are described in another paper in this issue[10]. In all, 14 sets of $\tau_{p\lambda}$ estimates are made on 14 clear days between 25 February 1998 and 28 March 1998, at 14 distinct locations over the Arabian Sea and southwest Indian Ocean on either side of the ITCZ. The distribution of these data samples are given in Table 1, where the entire data are put into three groups G-I, G-II and G-III; G-I and G-II pertaining to the oceanic regions north of the ITCZ and G-III to the pristine environment south of the ITCZ. G-I contains data collected during the onward leg, mainly along the coastal Arabian Sea and equatorial Indian Ocean closer to the Indian peninsula, while G-II contains data from the same oceanic regions, but much farther away from the peninsula, during the return leg of

§For correspondence. (e-mail: spl_vssc@vssc.org)

the cruise. These 14 sets of $\tau_{p\lambda}$ are the basic data for our study.

Retrieval of columnar size distribution

Columnar size distribution (CSD) of aerosols is retrieved from the $\tau_{p\lambda}$ estimates by numerical inversion of the integral equation for Mie scattering

$$\tau_{p\lambda} = \int_0^{TOA} \int_0^{\infty} \pi r^2 Q_{ext}(r, \lambda, m^*)\, n(r)\, dr\, dh, \quad (1)$$

where the integration is carried over all the relevant sizes of aerosols and over the entire atmosphere column (TOA-top of the atmosphere). In eq. (1), Q_{ext} is the Mie extinction efficiency parameter, which is a function of the particle radius r, wavelength of radiation λ, and the complex refractive index m^* of the aerosols; $n(r)$ is the size distribution function giving the number density of aerosols within a small radius range dr centred at r. Considering $n(r)$ as height invariant and replacing the size distribution $n(r)$ by the CSD, $n_c(r)$ is defined as

$$n_c(r)\, dr = \int_0^{TOA} n(r)\, dr\, dh. \quad (2)$$

Again, according to Mie theory only those particles having their size comparable with the interacting wavelength contribute significantly to Q_{ext} so that the limits of integration for r can be replaced with a finite range.

With these considerations eq. (1) becomes

$$\tau_{p\lambda} = \int_{r_1}^{r_2} \pi r^2 Q_{ext} n_c(r)\, dr, \quad (3)$$

where r_1 and r_2 are the lower and upper radii limits that contribute significantly to the integrand of eq. (3) and depend on the wavelengths over which $\tau_{p\lambda}$ are estimated. Eq. (3) is solved for $n_c(r)$ following the constrained linear inversion technique[11], as applied to the MWR data[12,13]. Wavelength-dependent refractive index values for marine aerosols as given by Shettle and Fenn[14] are used in evaluating Q_{ext} in eq. (3). The radius limits r_1 and r_2 are taken

Table 1. Group-wise distribution of the MWR database

Data group	Region of investigation	Location w.r.t the ITCZ	No. of data sets
G-I	Coastal Arabian Sea and equatorial Indian Ocean	North of ITCZ (onward leg)	5
G-II	Central Arabian Sea and equatorial Indian Ocean	North of ITCZ (return leg)	5
G-III	Pristine Indian Ocean	South of ITCZ	4

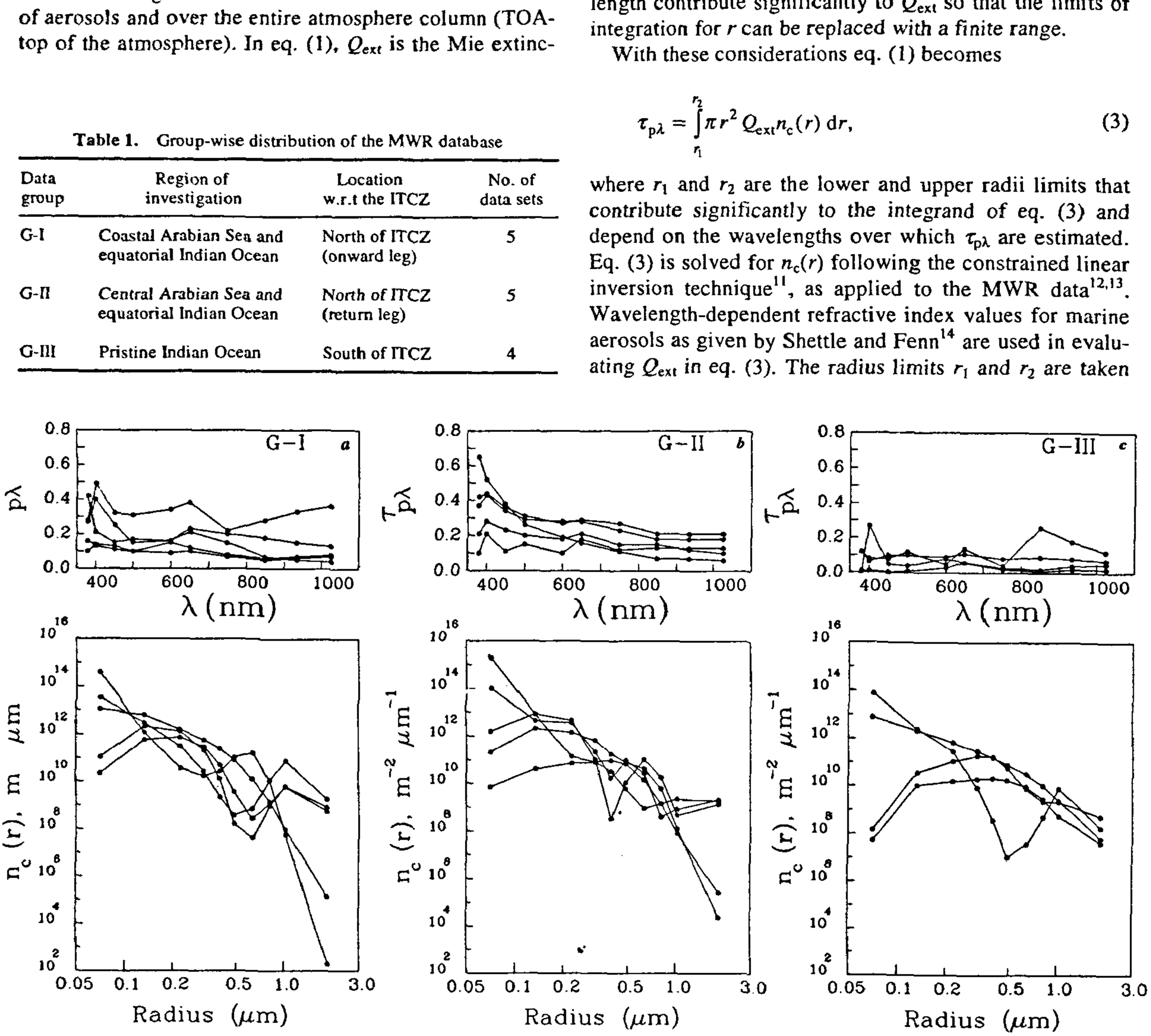

Figure 1 *a–c*. A composite representation of the $\tau_{p\lambda}$ values obtained using the MWR in the top panel and the CSDs retrieved from the $\tau_{p\lambda}$ in a log–log scale in the bottom panel for the data pertaining to *a*, G-I; *b*, same as (*a*) but for Central Arabian Sea data pertaining to G-II; *c*, same as (*a*) but for Indian Ocean regions south of the ITCZ pertaining to G-III.

as 0.05 and 3.0 μm respectively[7], based on estimations of the contribution to the kernel of eq. (3) for the extreme wavelengths (380 nm and 1025 nm) used in the MWR. Following this technique, all data sets (of $\tau_{p\lambda}$) are inverted to retrieve the CSDs for different oceanic regions and atmospheric conditions.

Results and discussion

The CSDs retrieved from the $\tau_{p\lambda}$ data sets (given in Table 1) are shown Figure 1 *a*, *b*, *c* for G-I, G-II and G-III respectively as composites. In each figure, the bottom panel shows the CSDs in a log–log scale and the top panel shows the $\tau_{p\lambda}$ values from which the CSDs are retrieved. The CSDs in G-I and G-II are generally bimodal with a secondary large-particle mode at ~ 1.0 μm preceded by a primary small-particle mode at ~ 0.05 to 0.1 μm, which at times is either explicit or is only indicated. Generally, these two modes are attributed to different source processes[3,7]; the primary mode is associated with the secondary processes, namely gas to particle conversion, condensation and coagulation, and the secondary mode to direct sea-spray production. On the other hand, the CSDs in G-III are generally unimodal with a broad peak at ≥ 0.5 μm, showing an near absence of the sub-micron primary mode. This suggests that a major portion of the sub-micron ($r < \sim 0.5$ μm) aerosols are associated with anthropogenic processes over the continent and are brought over to the ocean by the favourable northerly wind. However, they do not appear to pass across the ITCZ towards the south. In order to quantify the above points, the various aerosol parameters are evaluated from the CSDs. The columnar mass loading m_L is estimated as

$$m_L = \tfrac{4}{3}\pi\rho_a \int_{r_1}^{r_2} n_c(r)\,dr, \tag{4}$$

where $\rho_a = 2.2\ \mathrm{g\ cm^{-3}}$ is the density of marine aerosols. The effective radius R_{eff} is evaluated as the ratio of the total volume to area of the aerosols, according to the relation

$$R_{eff} = \frac{\int_{r_1}^{r_2} r^3 n_c(r)\,dr}{\int_{r_1}^{r_2} r^2 n_c(r)\,dr} \tag{5}$$

The columnar number density of aerosols N_t is evaluated as the area under the CSD curve

$$N_t = \int_{r_1}^{r_2} n_c(r)\,dr. \tag{6}$$

By dividing the CSD curves into two parts with $r = 0.5$ μm as a cut-off between the accumulation and coarse particles, the columnar concentration of accumulation mode aerosols (N_a) and of coarse (sea-spray) aerosols (N_c) are also estimated:

$$N_a = \int_{r_1}^{0.5} n_c(r)\,dr, \tag{7}$$

$$N_c = \int_{0.5}^{r_2} n_c(r)\,dr. \tag{8}$$

m_L is directly proportional to the total volume of aerosols and is more sensitive to changes in N_c, while R_{eff} is influenced by both N_a and N_c. The latitudinal variations of these parameters are given in Figures 2 and 3. In Figure 2 the aerosols concentrations, N_t, N_a and N_c are plotted from top to bottom in logarithmic scale while at the bottom-most panel the ratio of N_a to N_c is plotted again in logarithmic scale. This ratio measures the relative abundance of accumulation aerosols over the coarse ones. In all the panels, the points with solid circles correspond to regions north of the ITCZ which are under the influence of conti-

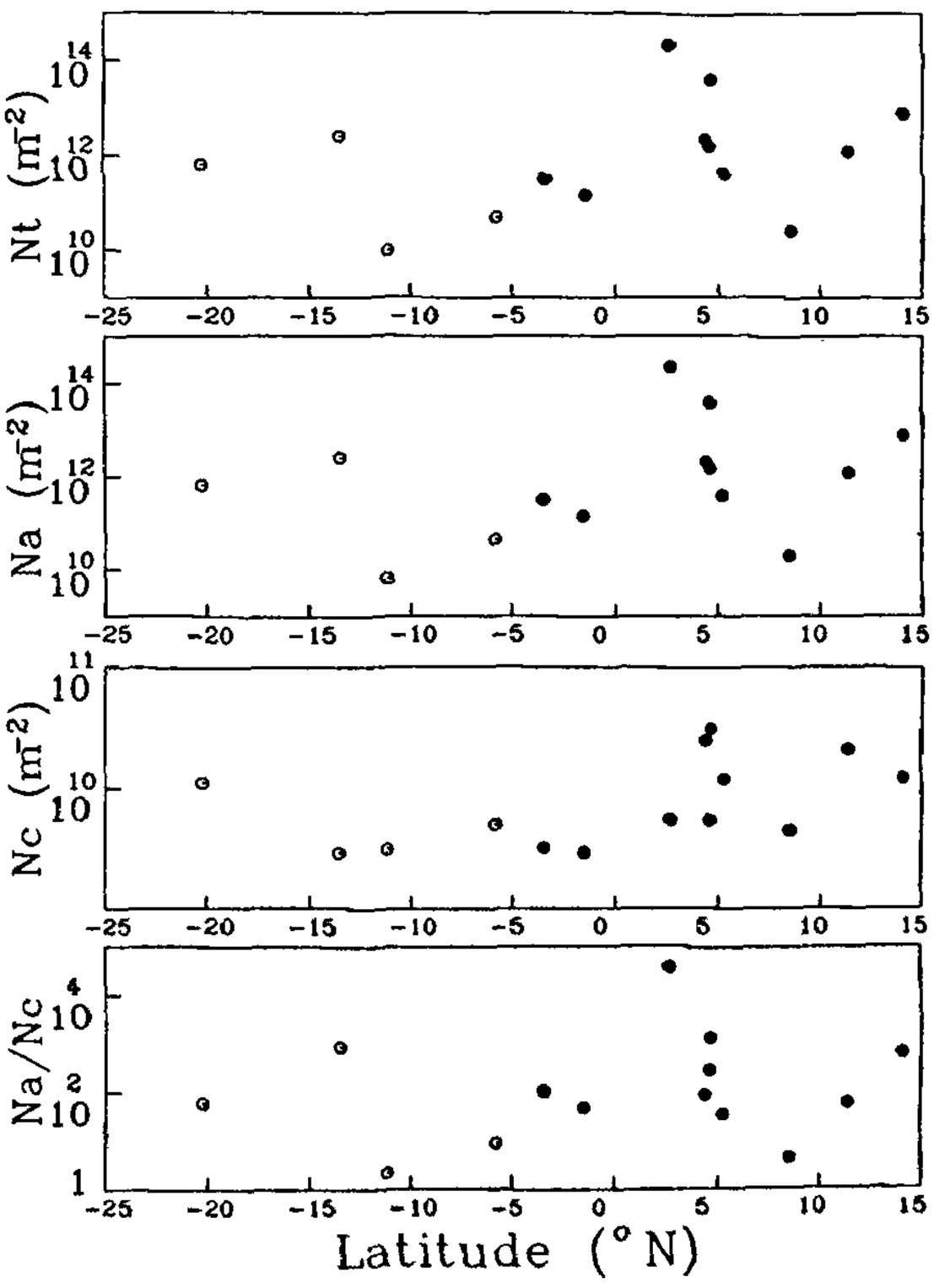

Figure 2. Latitudinal variation of derived number concentrations of aerosols. From top to bottom the panels show variations of N_t, N_a, N_c and N_a/N_c respectively.

nental air mass while the open circles correspond to locations south of the ITCZ. In Figure 3 the top panel shows the latitudinal variation of columnar mass loading m_L while that of R_{eff} is given in the bottom panel. The following features emerge:

(i) Towards the north of the ITCZ, both N_t and N_a are generally higher (by one to two orders of magnitude) than those on the south of the ITCZ.
(ii) The columnar contents of coarse aerosols remain generally around the same level (~ 10^{10} m^{-2}) except for the two cases near Male (4.6°N).
(iii) There is a near ten-fold increase in the concentration of accumulation particles on the northern side of the ITCZ.
(iv) Mass loading is higher close to the coast as well as in central Arabian Sea (in the northern hemisphere) and drops rapidly on south of the equator, falling by a factor of 5 south of the ITCZ.

The mean value of all these parameters is estimated for the sets in G-I, G-II and G-III separately and appears in Table 2. Clearly, the abundance of the accumulation particles increases substantially from the values on the south and this increase is remarkably large in the return leg over the central Arabian Sea, rather than closer to the Indian peninsula.

The effective radius is ~ 0.5 to 0.6 μm and nearly the same all over, while the mass loading is substantially lower south of the ITCZ. It is only moderately high near the coast while in the central Arabian Sea region (G-II) it is the highest. Examination of Figure 2 and 3 and Table 2 reveals that this high value of m_L is associated with the very large increase in N_a in G-II, rather than any abnormal changes in N_c. As N_c is mostly of marine origin, it is not expected to show any large scale changes when the wind speeds are low (4 to 5 ms^{-1}) as has been the case for G-II[10]. This is also borne out by Table 2 (column 4). Since there is no source over the central Arabian Sea to account for this enormously large increase in N_a, it is only possible that these fine aerosols are brought over the ocean by air trajectories.

This aspect has been examined in detail with the help of the real-time meteorological reanalysis atlas of the region, published by Jha and Krishnamurti[15]. Figure 4 displays the general synoptic pattern of the surface streamlines (taken from the atlas) during the period when the ship was sailing close to the Indian peninsula and Maldives (i.e. 23 to 28 February 1998), as represented by the three panels. The mean position of the ship on each day is marked by a rectangle in each panel. It can be seen that during this period the ship was under the strong influence of surface winds from the central Indian peninsula, and consequently the aerosol loading and τ_p remain high. As the heavier (large) particles would drop out fast by gravitational settling, the air parcels reaching the ship would be richer in sub-micron particles of continental origin (anthropogenic/natural). As a result, both N_a and N_a/N_c are quite high as can be seen from Figure 2 and Table 2 (G-I). As the ship moves further to the south Indian Ocean from 1 March onwards, the streamlines reaching the ship's environment become significantly different as can be seen from Figure 5, which is same as Figure 4 but for the period 1 to 6 March 1998. The streamlines reaching the ship have mainly originated from the north-east region of India and have travelled a considerably long distance over the Bay of Bengal before entering the southern Indian Ocean. During this travel, a large amount of (coarse) aerosols will have been lost over the ocean and the sub-micron aerosols would have become more aged and undergone microphysical processes enroute leading to

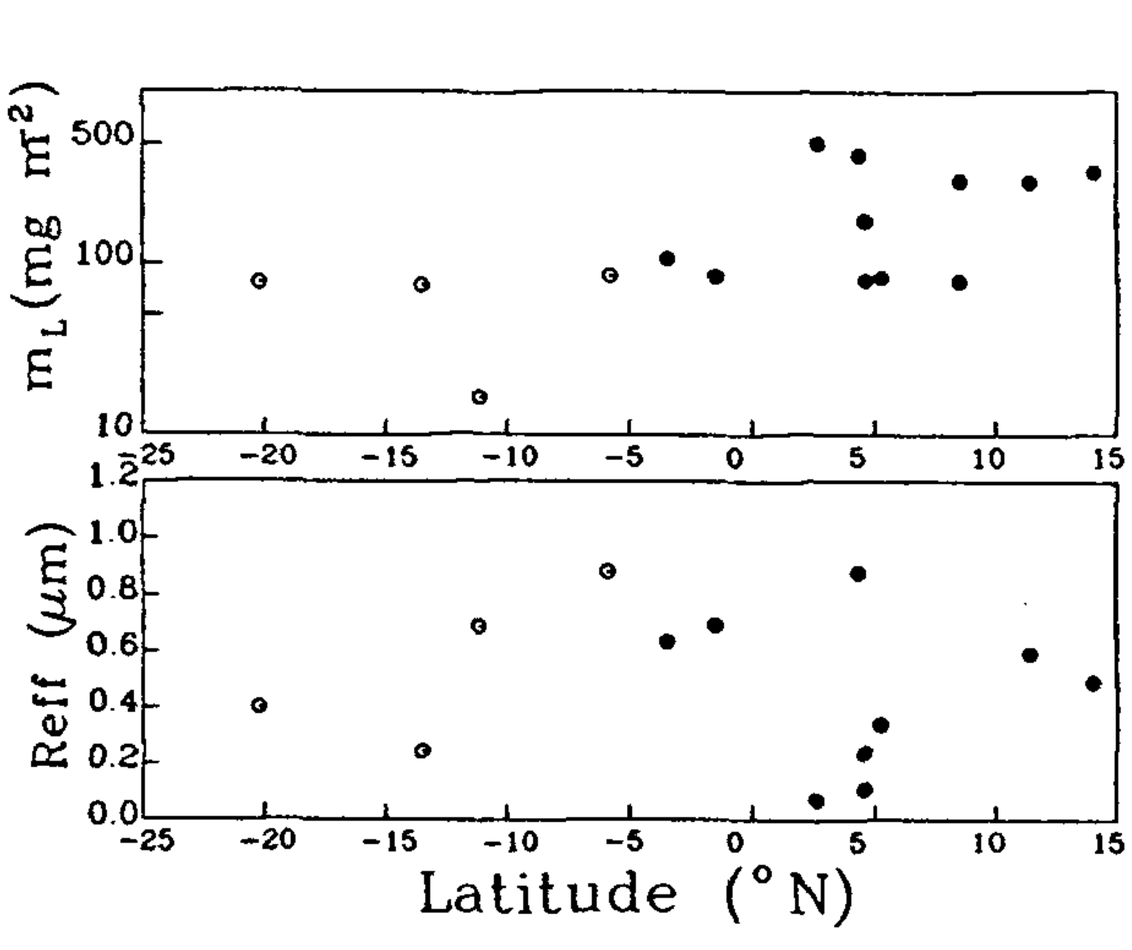

Figure 3. Latitudinal variation of columnar mass loading m_L and effective radius R_{eff}.

Table 2. Mean aerosol size parameters

Data group	Mean values of N_t $10^{12}(m^{-2})$	N_a $10^{12}(m^{-2})$	N_c (m^{-2})	N_a/Nc	R_{eff} (μm)	m_L (mg m^{-2})
G-I	8.8	8.65	1.35×10^{10}	641	0.51	175
G-II	44.2	43.82	1.09×10^{10}	3990	0.58	308
G-III	1.47	1.46	0.60×10^{10}	243	0.55	64

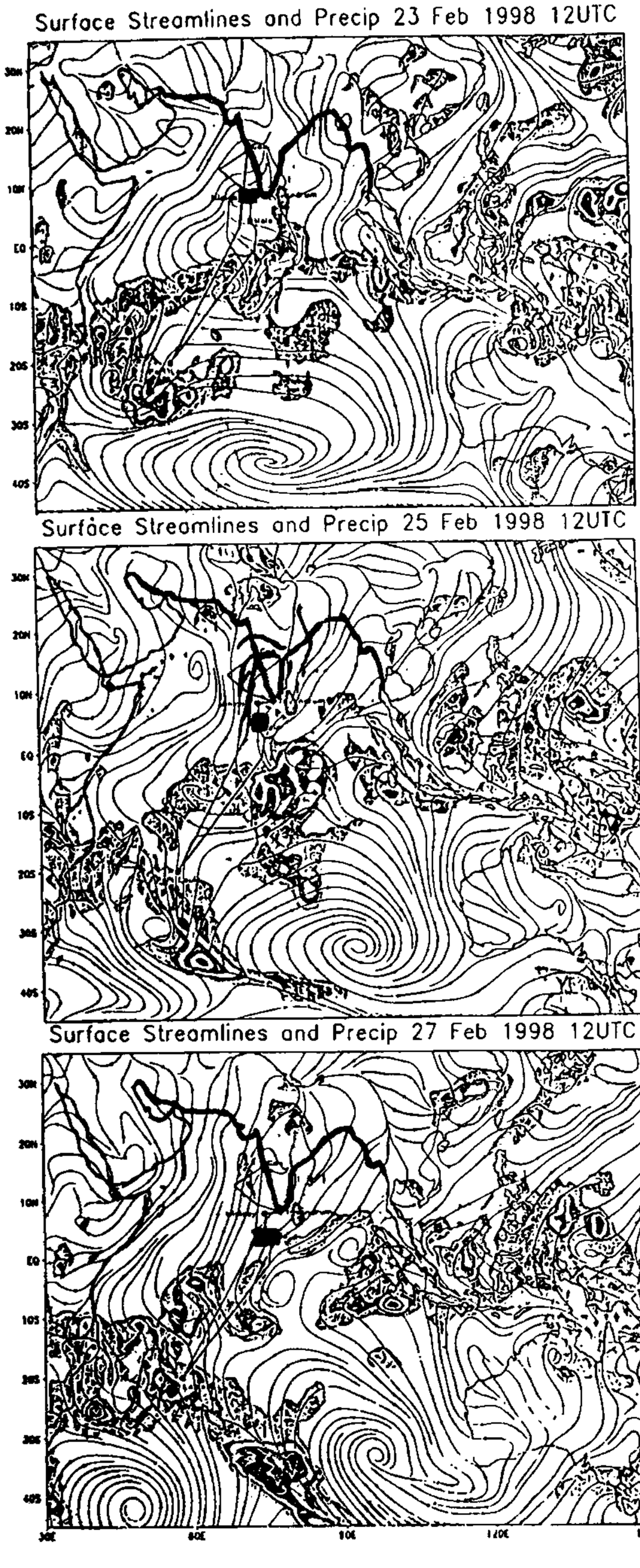

Figure 4. Surface streamlines over the INDOEX study area during 23–28 February 1998 (from Jha and Krishnamurthi[15]). The mean position of the ship is marked by a rectangle in each panel. The cruise tracks in the panels are only indicative and not to exact.

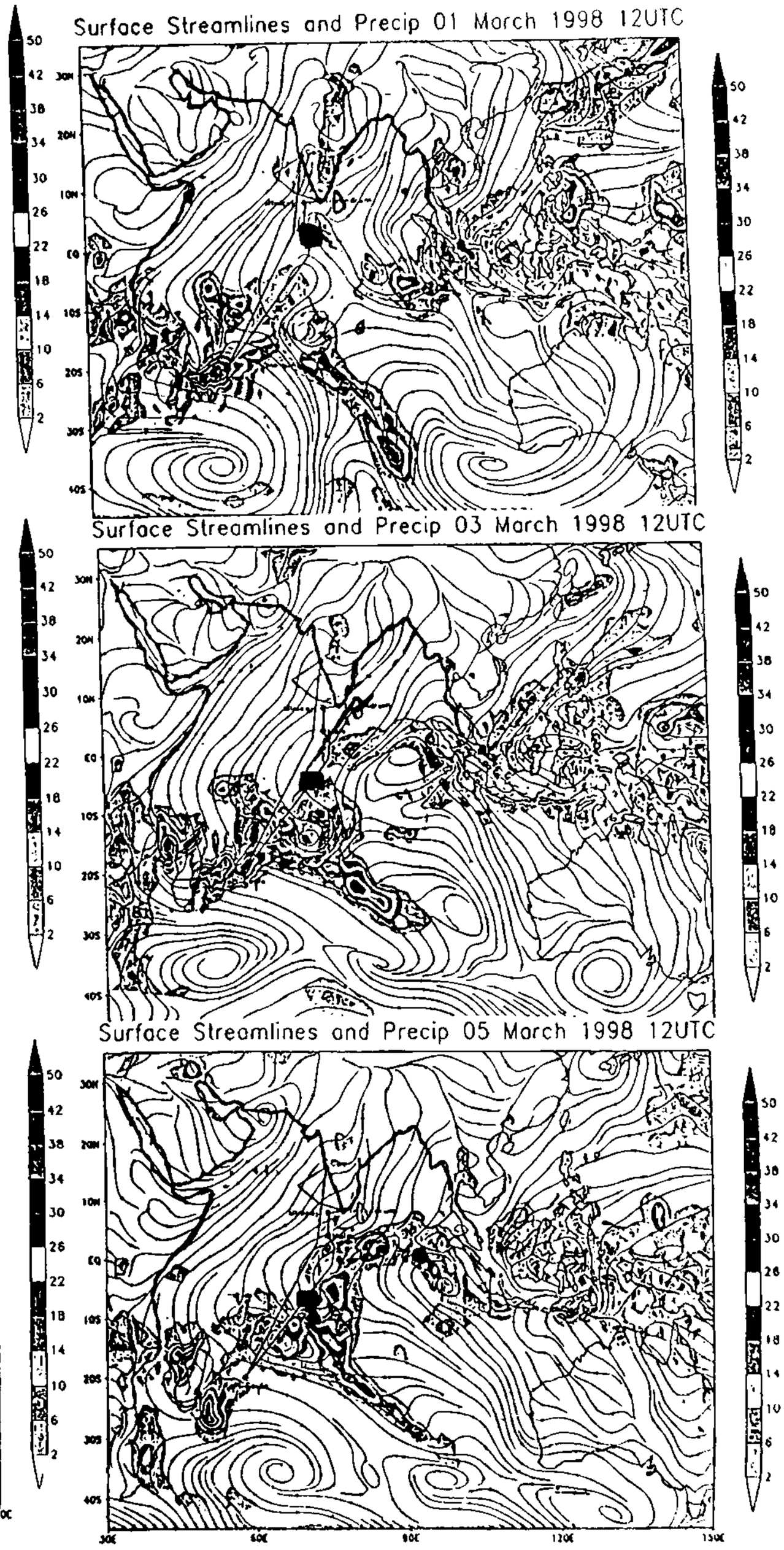

Figure 5. Same as Figure 4, but during 1–6 March 1998. The change in the streamlines reaching the ship is to be noted in particular (from ref. 15).

size transformation. Consequently the optical depth (Figure 1, top panel), mass loading (Figure 3, top panel), N_t (Figure 2, top panel) reduce, and the accumulation mode becomes pronounced (Figure 1, bottom panel). Note that coagulation significantly reduces the concentration of very small particles, and the resultant increase in the

concentration of large particles will be very small, so that N_t will decrease. The relative abundance of accumulation mode does not show significant change as accumulation particles have longer atmospheric lifetimes[2,16] and undergo only size transformation.

On the south of ITCZ (9 to 20 March 1998) the ship encountered mainly pure/clear pristine oceanic air coming from the S/S-E. As these air tracks are completely over the ocean (mid-latitude), they are not affected by anthropogenic activities; thus, there is a rapid decrease in N_a and

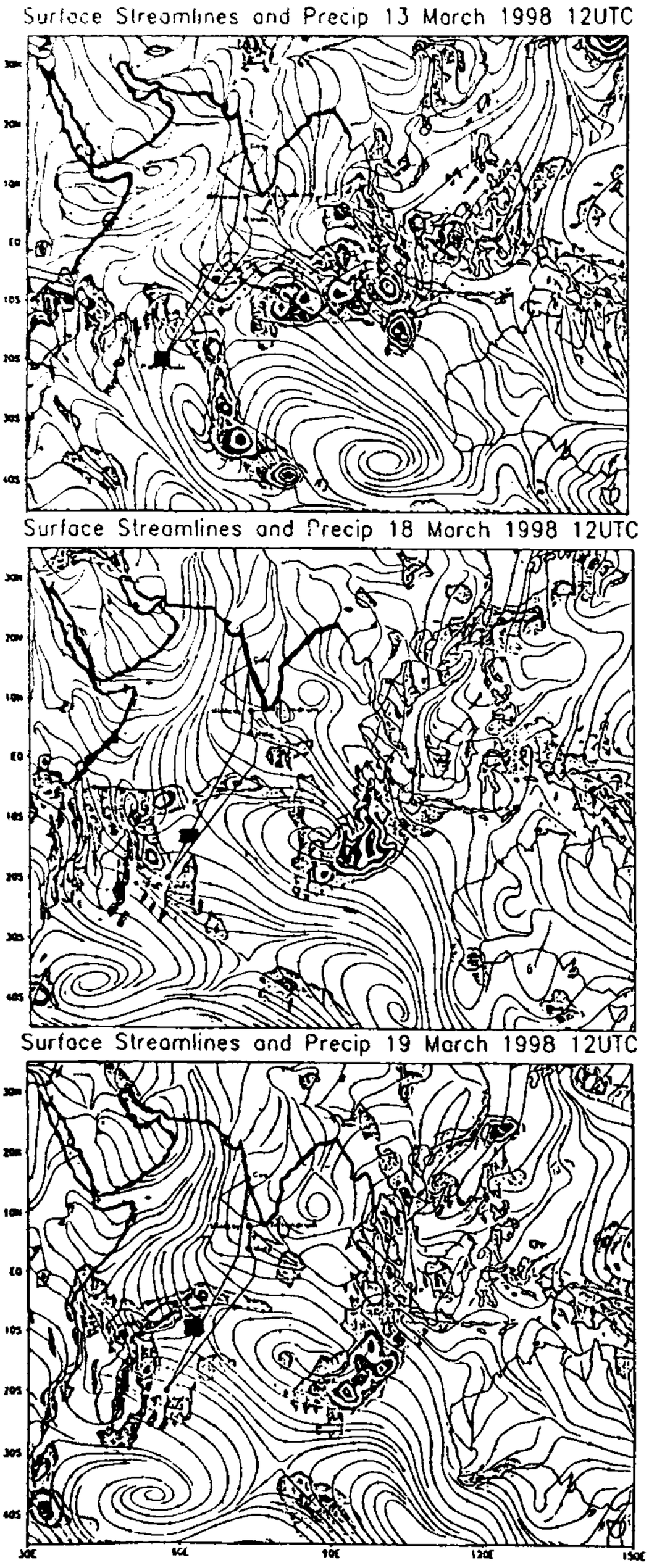

Figure 6. Same as in Figure 4, but for the region south of the ITCZ.

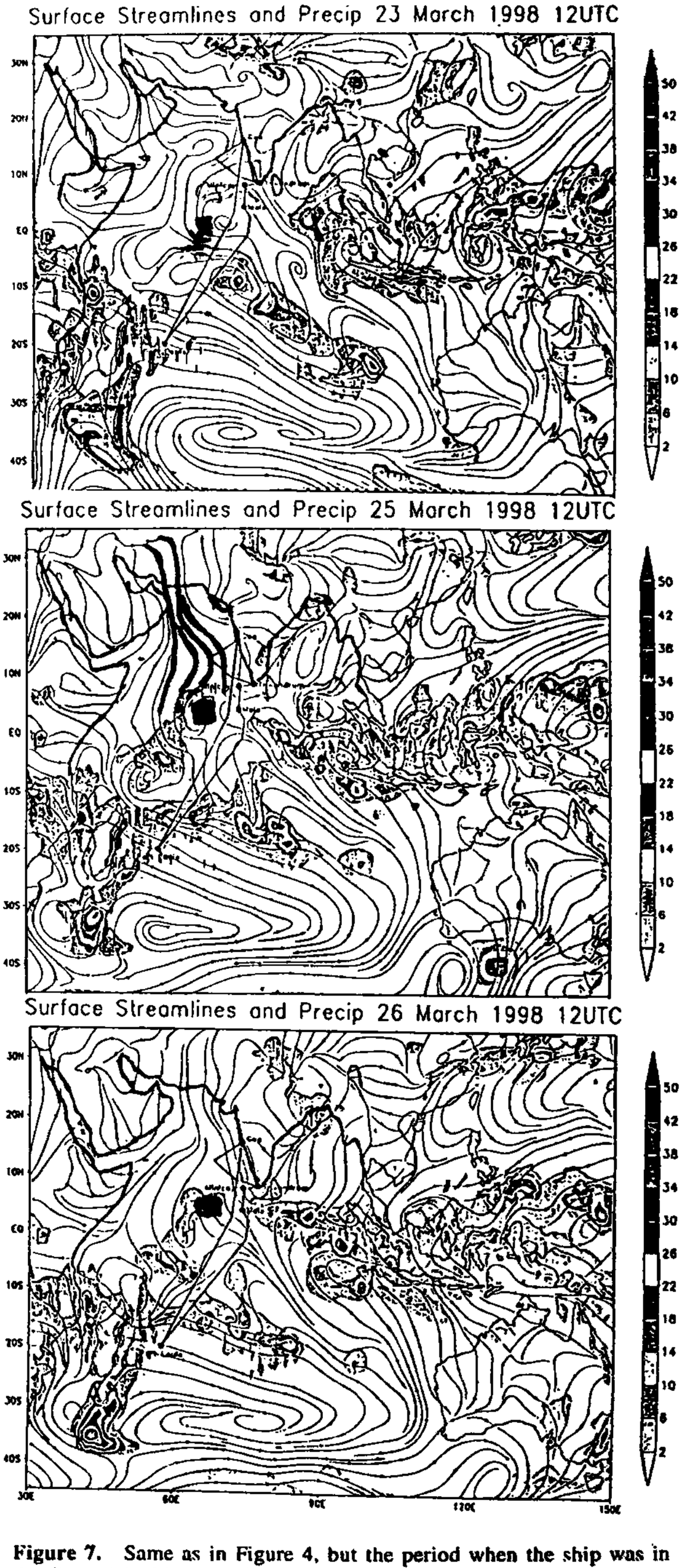

Figure 7. Same as in Figure 4, but the period when the ship was in the Central Arabian sea, during the return leg. Note that the streamlines reaching the ship are from west Asia and not from India.

N_a/N_c and τ_p at shorter wavelengths (as can be seen from Figures 2 and 1 *c*) because the τ_p at shorter wavelengths depend strongly on N_a. The course particle concentration does not differ much between G-I to G-III or G-III to G-II as be seen in Table 2. The substantial decrease in N_a and the aged nature of the aerosol reaching these regions lead to the broad unimodal type CSD observed generally in G-III (Figure 1 *c*, bottom panel).

On the return leg, there are two distinct streamlines as seen from Figure 7; one from the S-W oceanic region and the other from the north-west Asia. There is a substantial increase in τ_p (Figure 1 *b*, top panel) at $\lambda < 650$ nm, m_L. (Figure 3, top panel), N_t, N_a and N_a/N_c (Figure 2) associated with this. The CSDs become bimodal with a large primary mode at ~ 0.05 μm. As mentioned earlier, concerning the south of ITCZ, the southerly flows do not have large accumulation mode sub-micron particles. As such, the increase in N_a and N_a/N_c and N_t is mainly due to sub-micron particles brought over to the central Arabian Sea by the streamlines from the west Asian regions. It is quite possible that the fine mineral dust lifted from the arid areas of this region is transported by these streamlines. Thus, the mineral dust transport from the west Asian region may be a potential source of sub-micron aerosols over the central Arabian Sea, the effect of which can be comparable to, if not more than, the effect of aerosols transported from peninsular India to the near by coastal environment. The effect of this additional loading manifests an increase in the optical depths at the shorter wavelengths, seen over these regions and also as a substantial increase in the surface mass concentration observed by other independent aerosol measurements[17]. However, all these parameters as well as N_a register extremely low values south of the ITCZ. The ITCZ appears to act as a pseudo barrier which blocks the sub-micron aerosols from entering these pristine southern regions. The large (coarse) particles appear to be mainly of oceanic origin and their concentration remains nearly consistent throughout.

Conclusions

Our studies on the size characteristics of aerosols over the ocean have revealed the following.

(i) Over oceanic regions due north of the ITCZ, the size distributions of aerosols are generally bimodal with an accumulation mode at ~ 0.05 μm and a coarse particle mode at ~ 1.0 μm; both being attributed to different source processes. On the south of the ITCZ, the CSDs tend to become unimodal with a broad mode primarily due to coarse aerosols combined with the depleted and aged accumulation mode aerosols.

(ii) Transport of fine aerosols from West Asian region (west of India) causes high loading (of mass and concentration) of aerosols in the Central Arabian Sea, which is even higher than that caused by the continental air blowing over the peninsula, over the coastal regions adjacent to western India.

(iii) There is a significant depletion in the concentration as well as the relative abundance of accumulation mode aerosols on the south of the ITCZ (possibly due to the cut-off of the continental influence), while the concentration of coarse aerosols remains nearly the same through at the study area, suggesting them to be of mostly oceanic in origin.

1. Prospero, J. M., *J. Geophys. Res.*, 1979, **84**, 725–731.
2. Hoppel, W. A., Fitzgerald, J. W., Frick, G. M., Larson, R. E. and Mack, E. J., *J. Geophys. Res.*, 1990, **95**, 3659–3686.
3. Satheesh, S. K. and Moorthy, K. K., *Tellus*, 1997, **B49**, 417–428.
4. Satheesh, S. K., Moorthy, K. K. and Murthy, B. V. K., *J. Geophys. Res.*, 1998, **103**, 26183–26192.
5. Bergametti, G., Gomes, L., Coude-Gaussen, G., Rognon, P. and Le Couster, M. N., *J. Geophys. Res.*, 1989, **94**, 14855–14864.
6. Garrett, T. J. and Hobbs, P. V., *J. Appl. Meteorol.*, 1995, **52**, 2977–2983.
7. Moorthy, K. K., Satheesh, S. K. and Murthy, B. V. K., *J. Geophys. Res.*, 1997, **102**, 18827–18842.
8. Ramanathan, V., Crutzen, P. J., Coakley, J. A., Clarke, A., Collins, W. D., Dickerson, R., Fahey, D., Gandrud, B., Heymsfield, A., Kiehl, J. T., Kuettner, J., Krishnamurti, T. N., Lubin, D., Maring, H., Ogren, J., Prospero, J., Rasch, P. J., Savoie, D., Shaw, G., Tuck, A., Valero, F. P. J., Woodbridge E. L. and Zhang, G., *C⁴ Publication #162*, Scripps Institution of Oceanography, UCSD, California, 1996, pp 1–83.
9. Moorthy, K. K., Satheesh, S. K. and Murthy, B. V. K., *J. Atmos. Solar-Terr. Phys.*, 1998, **60**, 981–992.
10. Moorthy, K. K., Saha, A., Niranjan, K. and Pillai, P. S., *Curr. Sci.*, 1999, **76**, (this issue).
11. King, M. D., Byrne, D. M., Herman, B. M. and Reagan, J. A., *J. Atmos. Sci.*, 1978, **35**, 2153–2167.
12. King, M. D., *J. Atmos. Sci.*, 1982, **39**, 1356–1369.
13. Moorthy, K. K., Nair P. R. and Murthy, B. V. K., *J. Appl. Meteorol.*, 1991, **32**, 844–852. 1991.
14. Shettle, E. P. and Fenn, R. W., Environmental Research Paper No. 676, AFGL-TR-79-0214, Air Force Geophysics Laboratory, MA, 1979, pp. 26.
15. Jha, B. and Krishnamurti, T. N., Scientific Report, FSU 98-08, 1998.
16. Jaenicke, R., in *Aerosols and their Climatic Effects*, A. Deepak Publishing, USA, 1984, pp. 7–34.
17. Parameswaran, K., Nair, P. R., Rajan, R. and Ramana, M. V., *Curr. Sci.*, 1999, **76**, (this issue).

ACKNOWLEDGEMENTS. We thank the Department of Ocean Development and the National Institute of Oceanography for providing shipboard facilities.